Key Points:
- First polar view of Jupiter's auroral radio emissions
- Emissions composed of multiple V-shaped spectral features
- Juno passed close to or through five or more source regions

A new view of Jupiter's auroral radio spectrum

W. S. Kurth[1], M. Imai[1], G. B. Hospodarsky[1], D. A. Gurnett[1], P. Louarn[2], P. Valek[3,4], F. Allegrini[3,4], J. E. P. Connerney[5], B. H. Mauk[6], S. J. Bolton[3], S. M. Levin[7], A. Adriani[8], F. Bagenal[9], G. R. Gladstone[3,4], D. J. McComas[3,10], and P. Zarka[11]

[1]Department of Physics and Astronomy, University of Iowa, Iowa City, Iowa, USA, [2]IRAP, Toulouse, France, [3]Southwest Research Institute, San Antonio, Texas, USA, [4]Department of Physics and Astronomy, University of Texas at San Antonio, San Antonio, Texas, USA, [5]NASA Goddard Space Flight Center, Greenbelt, Maryland, USA, [6]Applied Physics Laboratory, The Johns Hopkins University, Laurel, Maryland, USA, [7]Jet Propulsion Laboratory, Pasadena, California, USA, [8]Istituto di Astrofisica e Planetologia Spaziali, INAF, Rome, Italy, [9]Laboratory for Atmospheric and Space Physics, University of Colorado Boulder, Boulder, Colorado, USA, [10]Department of Astrophysical Sciences and Office of the Vice President for the Princeton Plasma Physics Laboratory, Princeton University, Princeton, New Jersey, USA, [11]LESIA, Observatoire de Paris, Meudon, France

Abstract Juno's first perijove science observations were carried out on 27 August 2016. The 90° orbit inclination and 4163 km periapsis altitude provide the first opportunity to explore Jupiter's polar magnetosphere. A radio and plasma wave instrument on Juno called Waves provided a new view of Jupiter's auroral radio emissions from near 10 kHz to ~30 MHz. This frequency range covers the classically named decametric, hectometric, and broadband kilometric radio emissions, and Juno observations showed much of this entire spectrum to consist of V-shaped emissions in frequency-time space with intensified vertices located very close to the electron cyclotron frequency. The proximity of the radio emissions to the cyclotron frequency along with loss cone features in the energetic electron distribution strongly suggests that Juno passed very close to, if not through, one or more of the cyclotron maser instability sources thought to be responsible for Jupiter's auroral radio emissions.

1. Introduction

A primary objective of the Juno mission is the exploration of Jupiter's polar magnetosphere, and an essential element of this exploration is the in situ observations of processes associated with the generation of Jupiter's complex system of auroras that are the brightest in the solar system [*Bagenal et al.*, 2014]. As an element of Juno's "auroral suite" of instruments, the Waves radio and plasma wave instrument is designed to explore Jupiter's radio emissions and plasma waves that occur on auroral field lines in order to determine the roles they may play in the physics of Jupiter's auroras.

Jupiter was among the first sources observed by radio astronomers [*Burke and Franklin*, 1955]. Terrestrial observations provided early estimates of the strength of Jupiter's magnetic field under the assumption that the emissions were generated near $f_{ce} = 28|B|$, the local electron cyclotron frequency where frequency is in hertz and the magnetic field is in nanotesla. It is now known that auroral radio emissions are produced near f_{ce} by the cyclotron maser instability (CMI) [*Wu and Lee*, 1979]. The Voyager flybys showed that Jupiter's radio spectrum was complex and extended to 10 kHz and below [*Scarf et al.*, 1979; *Warwick et al.*, 1979]. See a review of Jovian radio emissions by [*Zarka*, 1998]. Other observations of Jovian radio emissions by spaceborne instrumentation were carried out by Ulysses, Galileo, and Cassini. These observations and an extensive collection of theoretical work provide the basis for Juno's exploration.

The Juno Waves instrument consists of an electric dipole antenna with a geometric effective length of 2.4 m parallel to the spacecraft *y* axis and perpendicular to Juno's spin axis, and a body-mounted search coil magnetometer whose sensitive axis is parallel to the spin axis. The Waves instrument collects electric spectra from 50 Hz to 40 MHz and magnetic spectra from 50 Hz to 20 kHz on a survey basis. For the measurements provided herein, the cadence was one spectrum every 2 s for frequencies below ~150 kHz until shortly after perijove. Subsequently and for frequencies above 150 kHz, the cadence was one spectrum per second. At preselected times, the Waves instrument can record, at a low duty cycle, waveforms that allow for higher temporal and spectral resolutions. An onboard algorithm can be used to select which of these are returned to the ground based on the broadband field strength computed for frequencies <150 kHz when there is insufficient telemetry to send all of them. For the highest frequencies, waveforms from an ~1 MHz band tuned to include f_{ce} are collected [*Kurth et al.*, 2017].
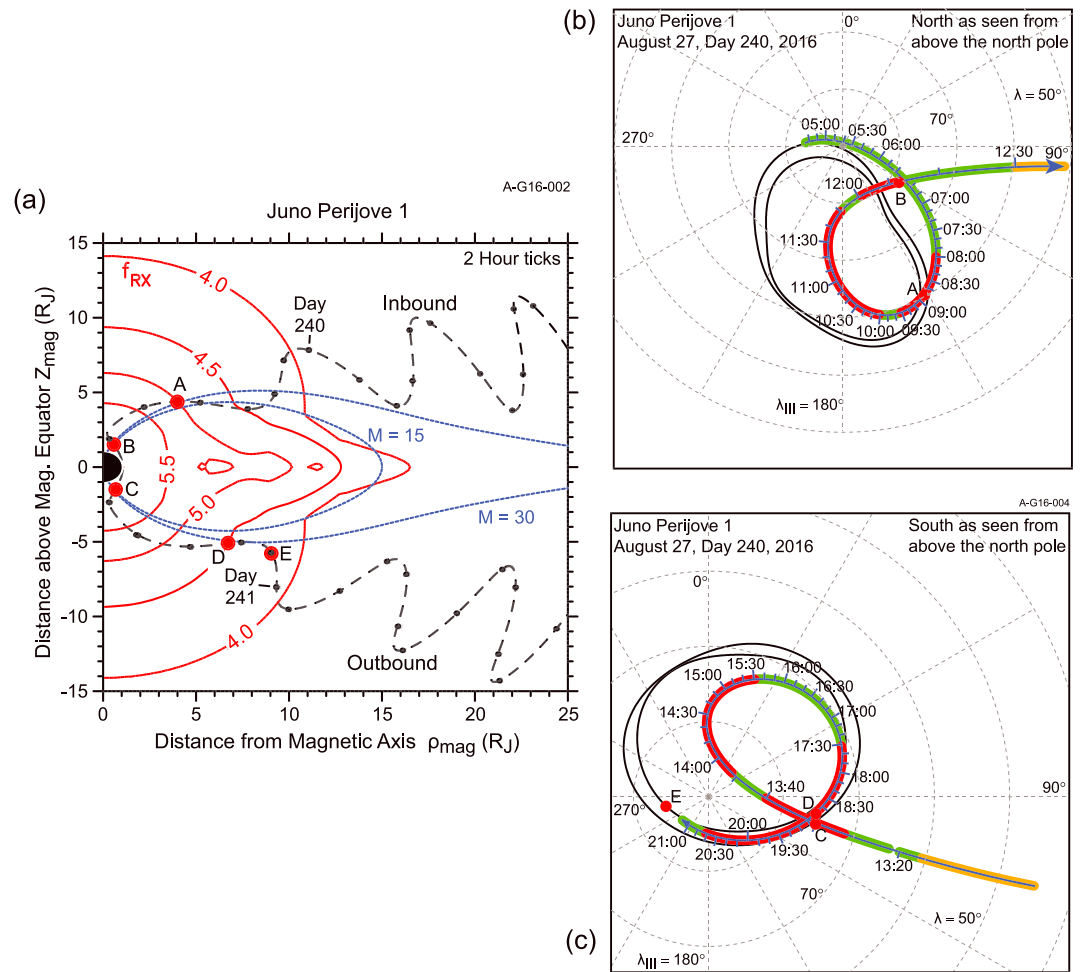
Figure 1. Geometry of Juno's first perijove. (a) A cylindrical projection of the flyby geometry using the VIP4 model. The trajectory is indicated with the black dashed line with 2 h ticks. The red contours are isosurfaces for the R-X cutoff with the log of the frequency indicated. Example VIP4 field lines with a disk current sheet [*Connerney et al.*, 1981] are shown in blue. The low-latitude R-X cutoff incorporates a modified plasma sheet density model [*Imai et al.*, 2017c]. The red dots indicate times when Juno passed through or close to auroral radio sources. (b) Projection of Juno's trajectory onto the northern hemisphere using the VIP4 model. The green color indicates times when the Waves instrument was in its survey mode, the red when burst mode was enabled, and the orange indicates a recorded segment of just the 20 kHz electric field channel. Note that an onboard algorithm is used to decide which data to retain for return to the ground so that actual burst coverage is not continuous. The double solid black lines indicate the statistical auroral oval from HST observations. (c) Same as Figure 1b but for the southern hemisphere as viewed from the north (through the planet).

The geometry of the perijove 1 trajectory is represented in two ways in Figure 1. First, the trajectory is shown in cylindrical magnetic coordinates based on the VIP4 dipole magnetic field model [*Connerney et al.*, 1998] in Figure 1a. The five red dots labeled A–E indicate times when Juno passed through or close to CMI radio sources as described below. Figures 1b and 1c show the footprint of the Juno trajectory mapped to the planet by using the VIP4 magnetic field model. The footprint starts in the north and ends in the south when Juno is about 10 R_J from Jupiter. Magnetic local time and Io phase change rapidly or even discontinuously at perijove. Figure S1 in the supporting information provides more detail on these variations.

2. Observations

Figure 2 shows the Juno Waves observations from 1 kHz to 30 MHz and from 08:00 on 27 August to 06:00 on 28 August, days 240 and 241, respectively, of 2016 (all dates and times herein are UT). The electric field spectral density is shown as a function of frequency and time using a gray scale. Note that the baseband portion of the High Frequency Receiver covering the frequency range from about 140 kHz to 3 MHz has reduced
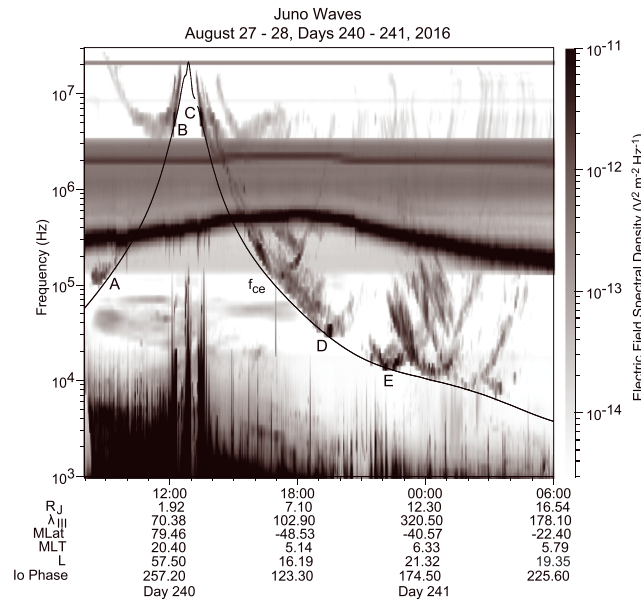
Figure 2. Frequency-time spectrogram showing electric field spectral density versus frequency and time using the gray scale on the right. The black trace indicates the electron cyclotron frequency. Possible source crossings are indicated by A–E which correspond to the same letters in Figure 1. The bands near 200 kHz, 2 MHz, and 20 MHz are interference.

sensitivity and two temperature-dependent noise lines that drift through this band near a few hundred kilohertz and 2 MHz. In spite of this, radio emissions in the hectometric band are visible. The black line represents the local f_{ce} based on the measured magnetic field intensity [*Connerney et al.*, 2017].

Figure 2 shows, for the first time from high latitudes, the full spectrum of Jupiter's auroral radio emissions from broadband kilometric radiation at a few tens of kilohertz, through hectometric radiation, and into the decametric band. Most of the emissions appear as V-shaped structures in frequency and time with the vertices occurring near f_{ce}, often with enhanced intensities. Some of the V-shaped structures appear to cover the full spectral range of the emissions. These emissions are not Io-related because Io's orbit phase with respect to Juno is not in the range expected for Io-related emissions [see, for example, *Carr et al.*,

1983]. At higher frequencies, the structures appear as vertex-early (like an opening parenthesis) and vertex-late arcs (like a closing parenthesis), commonly associated with decametric radiation. In the kilometric range, the bottoms of the V-shaped structures are likely the "bullseye" features observed by Ulysses [*Kaiser and MacDowall*, 1998].

We now examine the possibility that Juno passed through or very close to one or more CMI source regions during its first perijove pass. The times that we have examined are labeled A–E in Figure 2 and correspond to the red dots similarly labeled in Figure 1. Based on experience at Earth [*Roux et al.*, 1993; *Delory et al.*, 1998] and Saturn [*Lamy et al.*, 2010; *Kurth et al.*, 2011] as well as our understanding of the cyclotron maser instability [*Treumann*, 2006], we can look for a number of things in the observations that would point to a CMI source. First, a requirement for CMI is that $f_{ce} \gg f_{pe}$, where f_{pe} is the electron plasma frequency. Waves has found few spectral features during perijove 1 that provide a direct measure of f_{pe}. However, from near 8:00 to about 12:15 on day 240 *Tetrick et al.* [2017] have identified whistler mode emissions in the frequency range below a few tens of kilohertz. Near 12:12 and 13:30 there is evidence of funnel-shaped auroral hiss extending up to about 20 kHz. And, there are diffuse emissions we interpret as ordinary mode radio emissions above about 20 kHz near perijove as seen in Figure 2. All of these suggest that f_{pe} is well below f_{ce} in the polar magnetosphere.

Next, the cyclotron maser instability generates emissions at the relativistic f_{ce} or f_{ce}/γ, where γ is the Lorentz factor $(1 - v^2/c^2)^{-1/2}$, possibly corrected by a Doppler shift in the case of nonperpendicular propagation. The relevant speed v, here, is that of the resonant electrons driving the instability. Hence, we look for times where the radio emissions close to or just below f_{ce} as evidence of a source region. In Figure 3 we show an expanded frequency-time spectrogram for the event labeled B near 12:12 on day 240 with f_{ce} shown as the white trace. The Waves survey spectral resolution above 3 MHz is about 1 MHz; hence, it is difficult to accurately compare to f_{ce}. However, between 12:11 and 12:12 the 4–5 MHz channel shows a peak in intensity, while the bulk of this band is below the cyclotron frequency. Hence, this is a likely candidate for further examination. The radio emissions continue to be intense until about 12:16, although it is less clear how close their frequency is to f_{ce}. Note that while the burst mode was enabled (see Figure 1b), the onboard algorithm did not select data from this time.
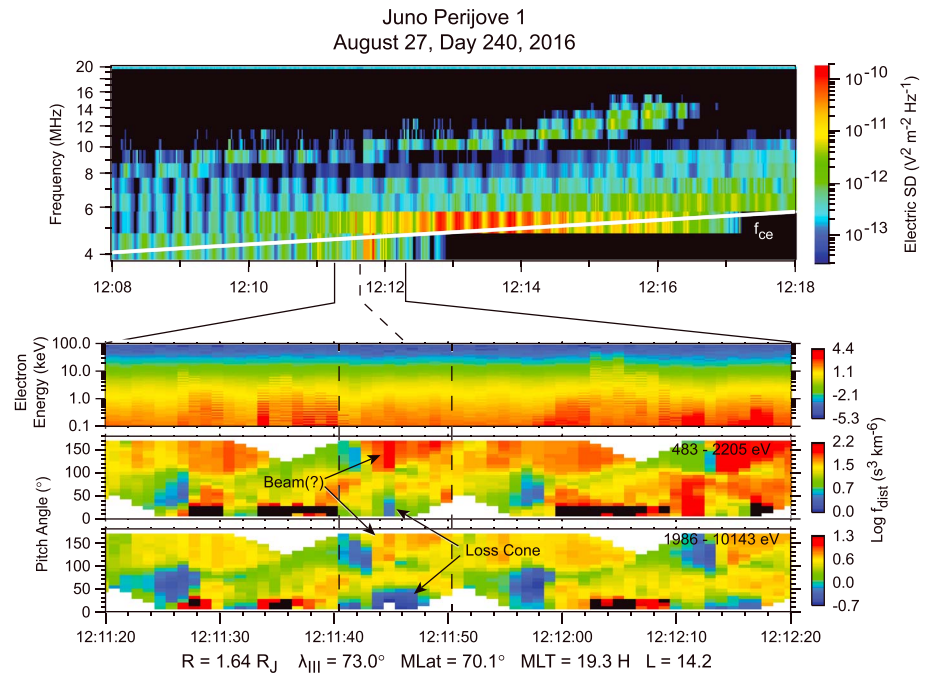
Figure 3. (top) Event B: Waves survey spectrogram showing enhanced radio emissions in the 4–5 MHz band. Bottom three plots: (top) Observations by the JADE electron instrument showing an energy-time spectrogram and two pitch angle distributions (middle) for ~0.5 to 2 keV electrons and (bottom) for ~2 to 10 keV electrons. For these northern polar distributions, 0° pitch angles are upgoing electrons and 180° pitch angles are downgoing particles.

Based primarily on in situ observations at Earth by Viking and FAST [*Delory et al.*, 1998; *Roux et al.*, 1993], we require a positive slope in the electron distribution perpendicular to the magnetic field as a source of free energy to drive the instability. Both a loss cone and a horseshoe-like distribution have been observed in terrestrial auroral kilometric source regions. In addition, the CMI emissions have been tightly tied to field lines threading active auroras, that is, with precipitating electrons, and presumably low-altitude acceleration regions. The Jovian Auroral Distributions Experiment (JADE) instrument [*McComas et al.*, 2013] provides high temporal resolution pitch angle distributions as shown in Figure 3 that are highly suggestive of such distributions. Near 12:11:45 the pitch angle distributions shown for 483–10,143 eV electrons show an enhanced loss cone and downgoing electrons, as one would expect. Note that over the northern hemisphere of Jupiter electrons with pitch angles near 180° are downgoing. It should be noted that the Jupiter Energetic particle Detector Instrument (JEDI) [*Mauk et al.*, 2014] also records loss cone distributions at higher energies at this time [*Mauk et al.*, 2017]. The JADE observations during this event are also discussed by *Allegrini et al.* [2017], who point out loss cone distributions in the interval from ~12:13 to 12:16.

Figure 4 shows evidence for another possible source, labeled C in Figure 2, now in the southern hemisphere. For this event Waves captured high-resolution measurements around 5 MHz which are shown in the figure with f_{ce} derived from magnetometer measurements superposed. The periodic nulls in the signal are due to the Waves antenna rotating at the ~2 rpm spin rate of Juno. The fine spectral structure is reminiscent of structure in other CMI emissions observed at Earth [*Gurnett et al.*, 1979], Saturn [*Kurth et al.*, 2005], and Jupiter [*Carr and Reyes*, 1999; *Ryabov et al.*, 2014]. These observations show that the hectometric emissions occur just above and even slightly below f_{ce} in this time interval, particularly near 13:30:20. The rising tone features well below f_{ce} from 13:28:45 to 13:29:20 and again around 13:30:20 are thought to be artifacts of the receiver response. Also shown in Figure 4 are JADE ion and electron energy spectra and electron pitch angle distributions. Here the ion spectrum suggests evidence for ion acceleration, a reasonable expectation on auroral field lines. The ion energy is as observed in the spacecraft frame since the spacecraft velocity of ~50 km/s translates only to order 10 eV. In the southern hemisphere, electrons near 0° pitch angle are precipitating. There is a period of enhanced downward going electrons near 13:29:40; the existence of a loss cone is unclear although present before and after this time. *Louarn et al.* [2017] show the electron distribution
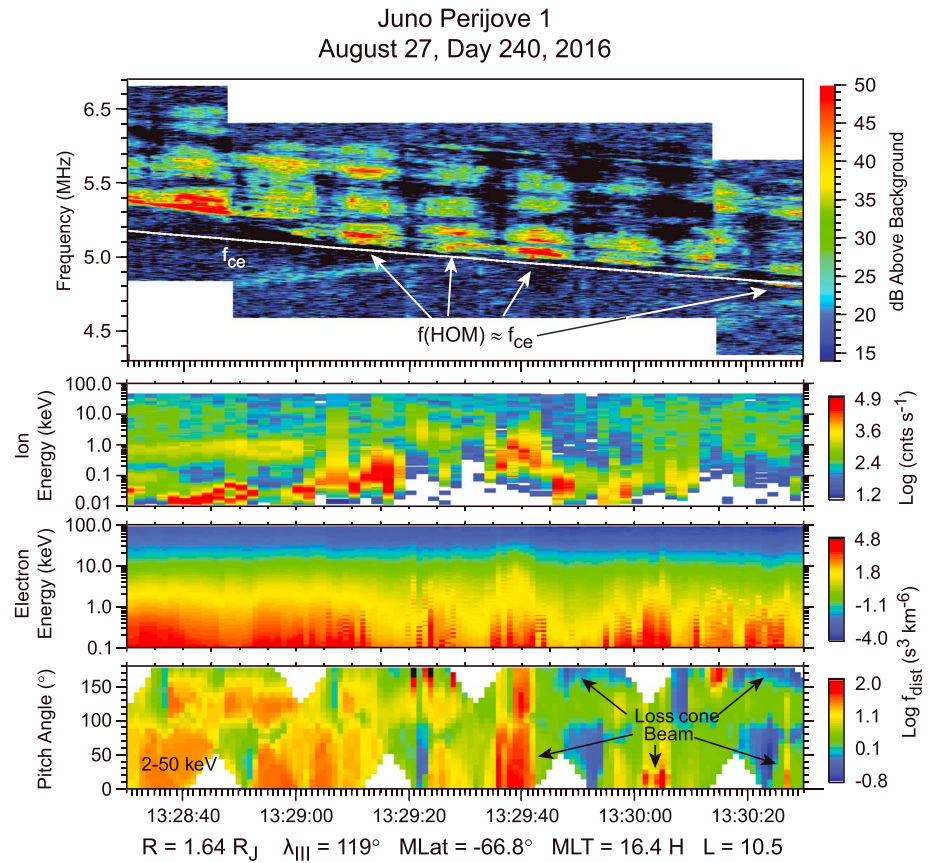
Figure 4. (top) Event C: High-resolution Waves spectrogram with arrows showing times when auroral radio emissions are very close to f_{ce} (white line). Bottom three plots: (top) An ion energy-time spectrogram showing evidence of ion acceleration to several keV. (middle) An electron energy-time spectrogram showing a power law-like distribution and (bottom) an electron pitch angle distribution with downgoing beams and loss cones for the upgoing electrons. Here at southern latitudes 0° pitch angles show downgoing electrons and 180° pitch angles show upgoing electrons.

function for this time and conclude that the loss cone is adequate to drive the CMI over the interval from about 13:27:40 to 13:29:10 and possibly to 13:29:40. Because of the Doppler shift, they would expect the emission ~200 kHz above f_{ce} at 13:28:50, similar to that seen early in Figure 4. Evidence for a loss cone during this time period is also found in the more energetic JEDI electrons.

Both events B and C near 12:12 and 13:30 show spectra extending to and even below f_{ce}, exhibit intensifications, and show downward going electron fluxes along with a loss cone for upward going electrons. All of these are suggestive of a local source for CMI emissions and in line with our expectations based on in situ observations at Earth.

Figure 2 highlights three other times when we suspect radio source crossings; these are identified as events A, D, and E. For these events, Juno was more distant from Jupiter; hence, the local f_{ce} was lower, and the radio sources in question are in what is traditionally called the kilometric wavelength range. Event A is a brief episode of broadband kilometric radiation occurring just above f_{ce} between 8:40 and 9:30 on day 240. There are no Waves burst data for this time period, and the survey data do not clearly show the radio emissions dropping below f_{ce}. However, near 8:48 JADE observes an increase in flux at 2–4 keV with a suggestion of a downgoing beam of electrons (not shown). There is insufficient evidence to identify this as a source crossing.

Event D occurs over an interval from about 18:00 to 19:40 on day 240, with a clear intensification centered on about 19:30. High-resolution data in Figure 5 show the extension of the radio emissions down to within 1 kHz or so of f_{ce} near 18:37. This spectrogram is also noteworthy as another example of spectral complexity in the radio emissions. The electron data during this period have not been examined for evidence of a free energy source for the CMI. Short of this analysis, we again classify this event as a close flyby of a source.
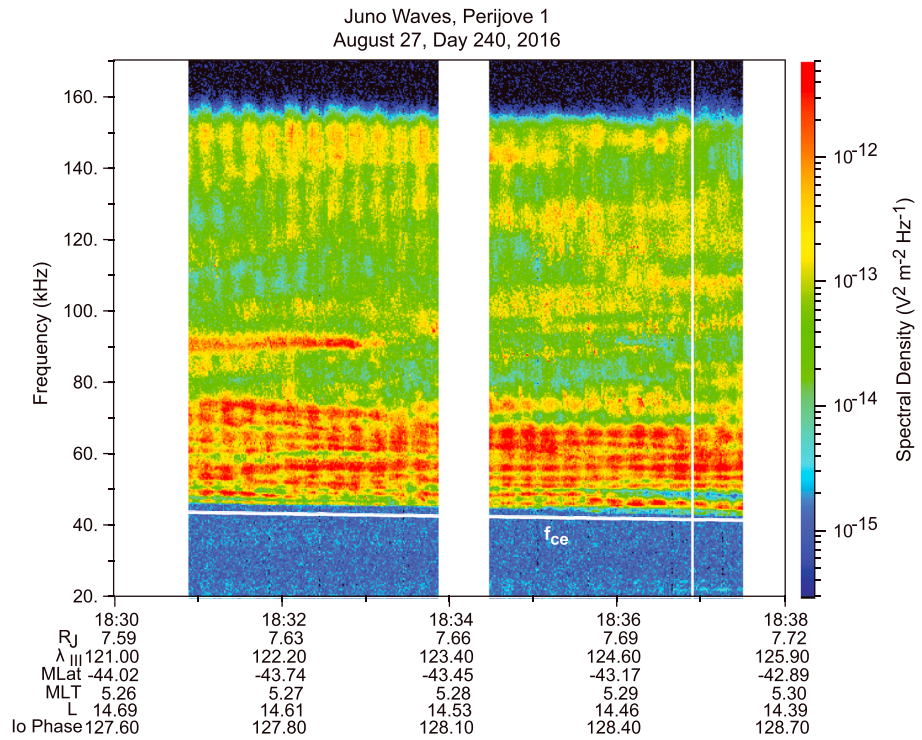
Figure 5. Event D. High-resolution Waves observations showing the extension of broadband kilometric radiation to close to f_{ce} and extensive frequency-time structure as is often seen for CMI emissions.

Event E extends from 21:20 to 22:40 on day 240. Here the Waves survey data clearly show the radio emission approaching f_{ce}. Near 21:24 and 21:58 f_{ce} lies in the middle of Waves survey channels with ~12% $\Delta f/f$ spectral resolution. The JADE observations show evidence for intense electron acceleration to energies of order 10 keV with an inverted-V signature [P. Louarn, personal communication, 2016]. At ~10 R_J from Jupiter, it is not clear whether JADE would be able to resolve a loss cone feature in the pitch angle distribution. Event E remains a good candidate for an in situ radio source.

3. Discussion and Summary

The Juno Waves observations from perijove 1 reveal an overall structure for non-Io-related Jovian auroral radio emissions that consists primarily of V-shaped emissions in frequency-time spectrograms in which the vertex falls close to the local electron cyclotron frequency where the emissions are generally more intense. The intensification and the proximity of the emission to f_{ce} provide the suggestion that at these times the spacecraft is close to a source region. For some of the events, closer inspection shows that the emission is at or even below f_{ce} and the electron distribution function sometimes shows downgoing beams and upgoing loss cones. *Louarn et al.* [2017] show that loss cone distributions observed in the vicinity of Event C are sufficient to drive the cyclotron maser instability. *Mauk et al.* [2017] report loss cone features in the more energetic electron observations made by the JEDI instrument at similar times as those of interest, here. Hence, it will be important to consider the full range of electron distributions before a final assessment of the distribution responsible for the radio emissions. We note, however, that for the possible sources noted in the present work, the fact that the radio emissions are not far below f_{ce} suggests that the resonant electrons cannot be much above the JADE electron energy range.

The V-shaped emissions observed are almost certainly the result of the relative motion of Juno with respect to CMI sources having thin conical sheet beaming patterns with large opening angles [*Kaiser and MacDowall*, 1998; *Queinnec and Zarka*, 1998]. There are V-shaped emissions both near AKR sources at Earth and Saturn, although these are typically filled as opposed to the narrow features in Figure 2. *Louis et al.* [2017] shows that some decametric emissions near Perijove 1 have V-shaped emissions that are well modeled by simulations. This suggests the V shape may be related to sources that are restricted to one or a small set of field lines.

Future work will include modeling the frequency-time structure with tools such as those described by *Louis et al.* [2017] and *Imai et al.* [2017a, 2017b].

While there are few specific spectral features that provide accurate plasma frequencies, it appears that f_{pe} is of order 20 kHz throughout the Jovian polar region, hence, $f_{ce} \gg f_{pe}$ for at least events B and C. The situation is similar to that at Saturn where the density is so low that there is no need for plasma cavities such as that occur over Earth's auroral regions to meet the $f_{ce} \gg f_{pe}$ requirement for the cyclotron maser instability.

Hess et al. [2008] examine various mechanisms by which electron acceleration events observed by the Galileo plasma instrument near Io might generate CMI emissions. Provided the plasma density in the source region is sufficiently low that Earth-like plasma cavities are not required, they favor an oblique instability driven by heating which generates emissions with beaming angles that vary along the Io flux tube with smaller angles at larger magnetic field strengths (lower altitudes, higher frequencies). While the emissions reported herein are not Io-related, it is likely similar conical beaming occurs.

The first examination of radio emissions from low altitude, high latitude with Juno provided an illuminating view of V-shaped frequency-time structures with vertices near f_{ce} and sometimes covering virtually the full spectral range from kilometric to decametric frequencies. Juno came at least close to up to five radio sources over about 18 h near closest approach. For some of the near-source crossings, electron observations at energies of a few to tens of keV show loss cone and beam features that are reminiscent of terrestrial auroral kilometric sources. *Louarn et al.* [2017] provide evidence that the distribution for Event C is sufficient to drive the cyclotron maser instability, consistent with the observed emissions. It remains to model the observed sources, as done by *Louis et al.* [2017] for Io-related emissions, to show that they can result in the V-shaped frequency-time structures and to further investigate the energetic electron distributions for their ability to drive the radio emissions. These observations, however, serve to confirm that the CMI process is a universal process for the generation of auroral radio emissions.

References

Allegrini, F., et al. (2017), Electron beams and loss cones in the auroral regions of Jupiter, *Geophys. Res. Lett.*, doi:10.1002/2017GL073180, in press.

Bagenal, F., et al. (2014), Magnetospheric science objectives of the Juno mission, *Space Sci. Rev.*, 1–69, doi:10.1007/s11214-014-0036-8.

Burke, B. F., and K. L. Franklin (1955), Observations of a variable radio source associated with the planet Jupiter, *J. Geophys. Res.*, *60*(2), 213–217, doi:10.1029/JZ060i002p00213.

Carr, T. D., and F. Reyes (1999), Microstructure of Jovian decametric S bursts, *J. Geophys. Res.*, *104*(A11), 25,127–25,141, doi:10.1029/1999JA900342.

Carr, T. D., M. D. Desch, and J. K. Alexander (1983), Phenomenology of magnetospheric radio emissions, in *Physics of the Jovian Magnetosphere*, edited by A. J. Dessler, pp. 226–284, Cambridge Univ. Press, New York.

Connerney, J. E. P., M. H. Acuna, and N. F. Ness (1981), Modeling the Jovian current sheet and inner magnetosphere, *J. Geophys. Res.*, *86*(Na10), 8370–8384, doi:10.1029/JA086iA10p08370.

Connerney, J. E. P., M. H. Acuna, N. F. Ness, and T. Satoh (1998), New models of Jupiter's magnetic field constrained by the Io flux tube footprint, *J. Geophys. Res.*, *103*(A6), 11,929–11,939, doi:10.1029/97JA03726.

Connerney, J. E. P., et al. (2017), Jupiter's magnetosphere and aurorae observed by the Juno spacecraft during its first polar orbits, *Science*, doi:10.1126/science.aam5928.

Delory, G. T., R. E. Ergun, C. W. Carlson, L. Muschietti, C. C. Chaston, W. Peria, J. P. McFadden, and R. Strangeway (1998), FAST observations of electron distributions within AKR source regions, *Geophys. Res. Lett.*, *25*(12), 2069–2072, doi:10.1029/98GL00705.

Gurnett, D. A., R. R. Anderson, F. L. Scarf, R. W. Fredricks, and E. J. Smith (1979), Initial results from the ISEE-1 and ISEE-2 Plasma Wave Investigation, *Space Sci. Rev.*, *23*(1), 103–122, doi:10.1007/BF00174114.

Hess, S., F. Mottez, P. Zarka, and T. Chust (2008), Generation of the Jovian radio decametric arcs from the Io flux tube, *J. Geophys. Res.*, *113*, A03209, doi:10.1029/2007JA012745.

Imai, M., W. S. Kurth, G. B. Hospodarsky, S. J. Bolton, J. E. P. Connerney, S. M. Levin, A. Lecacheux, L. Lamy, and P. Zarka (2017a), Latitudinal beaming of Jovian decametric radio emissions as viewed from Juno and the Nançay Decameter Array, *Geophys. Res. Lett.*, *44*, 4455–4462, doi:10.1002/2016GL072454.

Imai, M., W. S. Kurth, G. B. Hospodarsky, S. J. Bolton, J. E. P. Connerney, and S. M. Levin (2017b), Statistical study of latitudinal beaming of Jupiter's decametric radio emissions using Juno, *Geophys. Res. Lett.*, *44*, 4584–4590, doi:10.1002/2017GL073148.

Imai, M., W. S. Kurth, G. B. Hospodarsky, S. J. Bolton, J. E. P. Connerney, and S. M. Levin (2017c), Direction finding measurements of Jovian broadband and narrowband kilometric radiation from the Juno Waves instrument near perijove 1, *Geophys. Res. Lett.*, doi:10.1002/2017GL072850, in press.

Kaiser, M. L., and R. J. MacDowall (1998), Jovian radio "bullseyes" observed by Ulysses, *Geophys. Res. Lett.*, *25*(16), 3113–3116, doi:10.1029/98GL02255.

Kurth, W. S., G. B. Hospodarsky, D. A. Gurnett, B. Cecconi, P. Louarn, A. Lecacheux, P. Zarka, H. O. Rucker, M. Boudjada, and M. L. Kaiser (2005), High spectral and temporal resolution observations of Saturn kilometric radiation, *Geophys. Res. Lett.*, *32*, L20S07, doi:10.1029/2005GL022648.

Kurth, W. S., et al. (2011), A close encounter with a Saturn kilometric radiation source region, in *Planetary Radio Emissions VII*, edited by H. O. Rucker et al., pp. 75–86, Austrian Acad. of Sci., Vienna, Austria.

Kurth, W. S., G. B. Hospodarsky, D. L. Kirchner, B. T. Mokrzycki, T. F. Averkamp, W. T. Robison, C. W. Piker, M. Sampl, and P. Zarka (2017), The Juno Waves investigation, *Space Sci. Rev.*, doi:10.1007/s11214-017-0396-y, in press.

Lamy, L., et al. (2010), Properties of Saturn kilometric radiation measured within its source region, *Geophys. Res. Lett.*, *37*, L12104, doi:10.1029/2010GL043415.

Louarn, P., et al. (2017), Generation of the jovian hectometric radiation: First lessons from Juno, *Geophys. Res. Lett.*, *44*, 4439–4446, doi:10.1002/2017GL072923.

Louis, C. K., et al. (2017), Io-Jupiter decametric arcs observed by Juno/Waves compared to ExPRES simulations, *Geophys. Res. Lett.*, doi:10.1002/2017GL073036, in press.

Mauk, B. H., et al. (2014), The Jupiter Energetic Particle Detector Instrument (JEDI) investigation for the Juno mission, *Space Sci. Rev.*, *1–58*, doi:10.1007/s11214-013-0025-3.

Mauk, B. H., et al. (2017), Juno observations of energetic charged particles over Jupiter's polar regions: Analysis of mono-and bi-directional electron beams, *Geophys. Res. Lett.*, *44*, 4410–4418, doi:10.1002/2016GL072286.

McComas, D. J., et al. (2013), The Jovian Auroral Distributions Experiment (JADE) on the Juno mission to Jupiter, *Space Sci. Rev.*, 1–97, doi:10.1007/s11214-013-9990-9.

Queinnec, J., and P. Zarka (1998), Io-controlled decameter arcs and Io-Jupiter interaction, *J. Geophys. Res.*, *103*(A11), 26,649–26,666, doi:10.1029/98JA02435.

Roux, A., A. Hilgers, H. Deferaudy, D. Lequeau, P. Louarn, S. Perraut, A. Bahnsen, M. Jespersen, E. Ungstrup, and M. Andre (1993), Auroral kilometric radiation sources—In-situ and remote observations from Viking, *J. Geophys. Res.*, *98*(A7), 11,657–11,670, doi:10.1029/92JA02309.

Ryabov, V. B., P. Zarka, S. Hess, A. A. Konovalenko, G. Litvinenko, V. V. Zakharenko, V. A. Shevchenko, and B. Cecconi (2014), Fast and slow frequency–drifing millisecond bursts in Jovian decametric radio emissions, *Astron. Astrophys.*, *568*, A53, 11.

Scarf, F. L., D. A. Gurnett, and W. S. Kurth (1979), Jupiter plasma wave observations: Initial Voyager 1 overview, *Science*, *204*(4396), 991–995, doi:10.1126/science.204.4396.991.

Tetrick, S. S., D. A. Gurnett, W. S. Kurth, M. lmai, G. B. Hospodarsky, S. J. Bolton, J. E. P. Connerney, S. M. Levin, and B. H. Mauk (2017), Plasma waves in Jupiter's high latitude regions: Observations from the Juno spacecraft, *Geophys. Res. Lett.*, *44*, 4447–4454, doi:10.1002/2017GL073073.

Treumann, R. A. (2006), The electron-cyclotron maser for astrophysical application, *Astron. Astrophys. Rev.*, *13*, 229–315, doi:10.1007/s00159-006-0001-y.

Warwick, J. W., J. B. Pearce, A. C. Riddle, J. K. Alexander, M. D. Desch, M. L. Kaiser, J. R. Thieman, T. B. Carr, S. Gulkis, and A. Boischot (1979), Voyager 1 Planetary Radio Astronomy observations near Jupiter, *Science*, *204*(4396), 995–998, doi:10.1126/science.204.4396.995.

Wu, C. S., and L. C. Lee (1979), A theory of the terrestrial kilometric radiation, *Astrophys. J.*, *230*, 621–626, doi:10.1086/157120.

Zarka, P. (1998), Auroral radio emissions at the outer planets: Observations and theories, *J. Geophys. Res.*, *103*(E9), 20,159–20,194, doi:10.1029/98JE01323.